The following publication Qiu, W., Wang, X., Chen, Y., Fu, Q., Su, M., Zhang, L., ... & Zheng, H. (2016). Modulated excitation imaging system for intravascular ultrasound. IEEE Transactions on Biomedical Engineering, 64(8), 1935-1942 is available at https://doi.org/10.1109/TBME.2016.2631224.

A Modulated Excitation Imaging System for Intravascular Ultrasound

Weibao Qiu, Xingying Wang, Yan Chen, Qiang Fu, Min Su, Lining Zhang, Jingjing Xia, Jiyan Dai, Yaonan Zhang, Hairong Zheng

***Abstract*—Advances in methodologies and tools often lead to new insights into cardiovascular diseases. Intravascular ultrasound (IVUS) is a well-established diagnostic method that provides high-resolution images of the vessel wall and atherosclerotic plaques. High-frequency (>50 MHz) ultrasound enables the spatial resolution of IVUS to approach that of optical imaging methods. However, the penetration depth decreases when using higher imaging frequencies due to the greater acoustic attenuation. An imaging method that improves the penetration depth of high-resolution IVUS would therefore be of major clinical importance. Modulated excitation imaging is known to allow ultrasound waves to penetrate further. This paper presents an ultrasound system specifically for modulated-excitation-based IVUS imaging. The system incorporates a high-voltage waveform generator and an image processing board that are optimized for IVUS applications. In addition, a miniaturized ultrasound transducer has been constructed using $Pb(Mg_{1/3}Nb_{2/3})O_3$-$PbTiO_3$ (PMN-PT) single crystal to improve the ultrasound characteristics. The results show that the proposed system was able to provide increases of 86.7% in penetration depth and 9.6 dB in the signal-to-noise ratio for 60 MHz IVUS. *In vitro* tissue samples were also investigated to demonstrate the performance of the system.**

***Index Terms*—Ultrasound imaging, Intravascular ultrasound, Modulated excitation, High frequency ultrasound, Ultrasound system.**

I. Introduction

Intravascular ultrasound (IVUS) is a well-established diagnostic method that provides high-resolution images of vessel walls and atherosclerotic plaques [1]. IVUS has had a profound impact on clinical assessments, including morphological measurements of plaques [2] and guidance during stent placement [3, 4]. A vulnerable plaque typically consists of a lipid-rich necrotic core and a unique morphological feature of a thin fibrous cap [5]. In addition, neovascularization of a plaque is recognized as an indication of vulnerability [6]. The methodologies for measuring the composition of the necrotic core and the thickness of the fibrous cap, as well as for visualizing microvessels are of great clinical interest. The implementation of elastography for IVUS to measure the local mechanical properties in an atherosclerotic plaque to identify fibrous and fatty tissues [7]. Furthermore, virtual histology has been used to characterize the composition of plaques [8].

Traditional IVUS technology uses ultrasound with a center frequency of 20–45 MHz, but the resulting imaging spatial resolution makes it impossible to delineate the thin cap or microvessels. A multimodality intravascular imaging method combining ultrasound with optical coherence tomography (OCT) was employed to improve both imaging resolution and penetration [9], but this had the disadvantage of the high costs of the catheter and the overall system.

Recent progress of novel IVUS imaging techniques have been proposed using micromachined 1-3 composite [10,11], and dual frequency IVUS acoustic angiography [12,13]. In addition, high-frequency ultrasound was proposed for improving the imaging resolution of the IVUS method [14]. Increasing the ultrasound frequency to more than 100 MHz enables the resolution of IVUS to approach that of optical imaging methods. This means that IVUS could be an alternative and cost-effective solution to replace OCT-based intravascular imaging. However, the penetration depth is sacrificed because the acoustic attenuation in the tissue increases with the ultrasound frequency. An imaging method for improving the depth of penetration would be of major clinical interest.

It has been demonstrated that modulated excitation imaging can increase the penetration depth by elongating the ultrasound wave [15, 16], which extends the view for acquiring structural information of vessel walls [17, 18]. In addition, contrast-enhanced imaging with modulated excitation was proposed for visualizing the vasa vasorum using a conventional IVUS catheter [19]. The vulnerability of the plaque could be quantified by the microvasculature within the plaque in the presence of ultrasound microbubbles. Moreover, the

Manuscript received May 09, 2016. This work was supported by the National Science Foundation Grants of China (61302038, 81527901, 11325420, and 11534013), National Basic Research Program of China (2015CB755500), Research project of CAS (Y650311C31, QYZDB-SSW-JSC018), Guangdong Innovative and Entrepreneurial Research Team Program (2013S046), Natural Science Foundation of Guangdong Province (2015A030306018, 2014A030313686 and 2014A030312006), Shenzhen Peacock Plan (20130409162728468), Shenzhen International Collaboration Grant (GJHZ20140417113430615), and the Foundation Grants of Shenzhen (JCYJ20140610151856707).

W. Qiu*, X. Wang, Q. Fu, M. Su, L. Zhang, J. Xia, and H. Zheng* are with Paul C. Lauterbur Research Center for Biomedical Imaging, Shenzhen Institutes of Advanced Technology, Chinese Academy of Sciences, Shenzhen 518055, China (corresponding authors: wb.qiu@siat.ac.cn, hr.zheng@siat.ac.cn).

Y. Chen and J. Dai are with Department of Applied Physics, The Hong Kong Polytechnic University, Hong Kong.

Y. Zhang is with College of Electronics and Information Engineering, Xi'an Siyuan University, Xi'an 710038; Q. Fu, L. Zhang, and Y. Zhang are with Sino-Dutch Biomedical and Information Engineering School, Northeastern University, Shenyang 110169, China.

signal-to-noise ratio (SNR) was increased by the application of modulated excitation to pulse-inversion tissue harmonic imaging [20]. The modulated-excitation-based IVUS (ME-IVUS) imaging technique could increase the efficacy of ultrasound in assessments of cardiovascular diseases.

However, no previous study has specifically applied high-frequency (>50 MHz) ultrasound to improve the penetration depth in IVUS. Moreover, no study has proposed a design for a bespoke ME-IVUS system. Published studies of modulated excitation imaging have mostly implemented systems that combine different equipment such as commercial functional generators (from suppliers such as Agilent Technologies, Santa Clara, CA, and B&K Precision Instruments, Yorba Linda, CA) and power amplifiers (from suppliers such as Electronics and Innovation, Rochester, NY and Amplifier Research Corporation, Souderton, PA) [17–20]. These evaluation setups were noisy, bulky, and expensive, and so an ultrasound system specifically optimized for ME-IVUS still needs to be developed.

In this paper we propose an ultrasound system specifically designed for ME-IVUS. An arbitrary-waveform generator was developed using a power amplifier with a custom-built circuit for switching it off. A digital-to-analog converter (DAC) and data acquisition circuitry were incorporated for pulse generation and data processing. In addition, two miniaturized ultrasound transducers were constructed using $Pb(Mg_{1/3}Nb_{2/3})O_3$-$PbTiO_3$ (PMN-PT) single crystal. The methodology of the ultrasonic system is described in detail in the Section II. A description of the system hardware and an evaluation of the imaging depth are presented in Section III. Finally, the performance of the proposed system and potential applications are discussed in Section IV.

II. Methods

Fig. 1 shows a block diagram of the proposed imaging system design especially for ME-IVUS applications. A field-programmable gate array (FPGA) device was incorporated for waveform generation and image processing. A high-speed DAC and a linear power amplifier were designed for the generation of an arbitrary waveform with a high voltage and adjustable amplitude and phase. A transmit/receive switch allowed the transducer to be triggered, and echo signals from the transducer were acquired with high-speed data acquisition circuitry (i.e., FPGA, analog-to-digital converter [ADC], filter, and amplifier). A universal serial bus (USB) was employed for transferring data to a computer. The FPGA also synchronously controls the motor to rotate the rotational stage for sectional imaging of the tissue. The interface software for reconfiguration and operation of the imaging platform was written in the Visual C++ language.

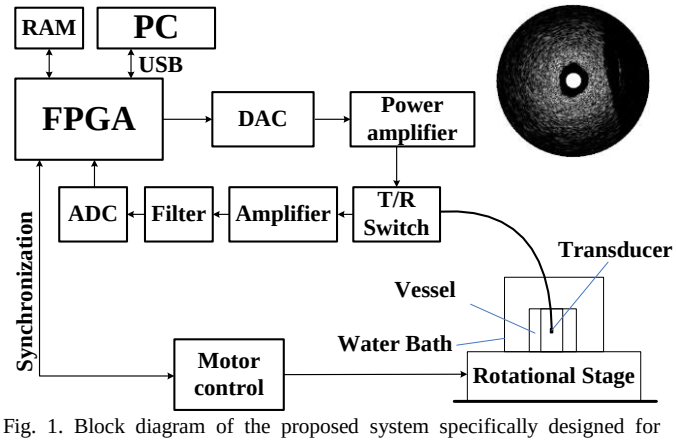

Fig. 1. Block diagram of the proposed system specifically designed for ME-IVUS imaging.

A. Waveform Generator

A waveform generator was developed for waveform generation with programmable parameters including its frequency, amplitude, and phase. An FPGA (Cyclone-V 5CGXFC7D7F31C8N, Altera Corporation, San Jose, CA) was employed as the central processor for waveform management and user interface. A DAC (DAC5682Z, Texas Instruments, Dallas, TX) with a maximum sampling rate of one Giga samples/ per second (GSPS) was employed to convert the digital signals into analog signals. The power amplifiers comprised two stages with a total gain of 40 dB. The waveform was first amplified by a low-voltage amplifier (THS3091, Texas Instruments), followed by a power amplifier, as shown in Fig. 2. A lateral double-diffused metal-oxide semiconductor technology power transistor (BLF578, NXP Semiconductors, Eindhoven, Netherlands) was employed for power amplification. The power amplifier worked in a pulsed mode. A circuit shown in Fig. 2(b) was used to control when the power amplifier was switched off. A MOSFET (metal-oxide semiconductor field-effect transistor) driver (MAX4420, Maxim Integrated, San Jose, CA) was utilized in the switching-off circuit. The output power was shut down immediately after the waveform had been generated. The noise generated by the power amplifier was blocked by the data acquisition circuitry, which ultimately improved the SNR of the images. In addition, the power consumption was decreased significantly, which eliminated the need for a heat sink in the power amplifier.

B. Data Acquisition Circuitry

In the data acquisition circuitry, a low-noise amplifier (AD8331, Analog Devices, Canton, MA) was used to amplify the echo signals. The gain was set to 50 dB during the data acquisition process. An analog filter was designed for antialiasing filtering to remove higher frequency noise. A 12-bit ADC (AD9230, Analog Devices) with a maximum sampling rate of 250mega-samples per second (MSPS), was employed to digitize the analog signals. The digitized signals were transferred to the FPGA via a low-voltage differential signaling interface. The FPGA was employed for high-speed signal processing and for implementing programmable algorithms such as for the bandpass filter, suppression filter, Hilbert transform, and envelope detection. A DDR3 SDRAM (MT41J128M16HA, Micron Technology, Boise, ID) was used as a data buffer. A clock generator (CDCM61002, Texas

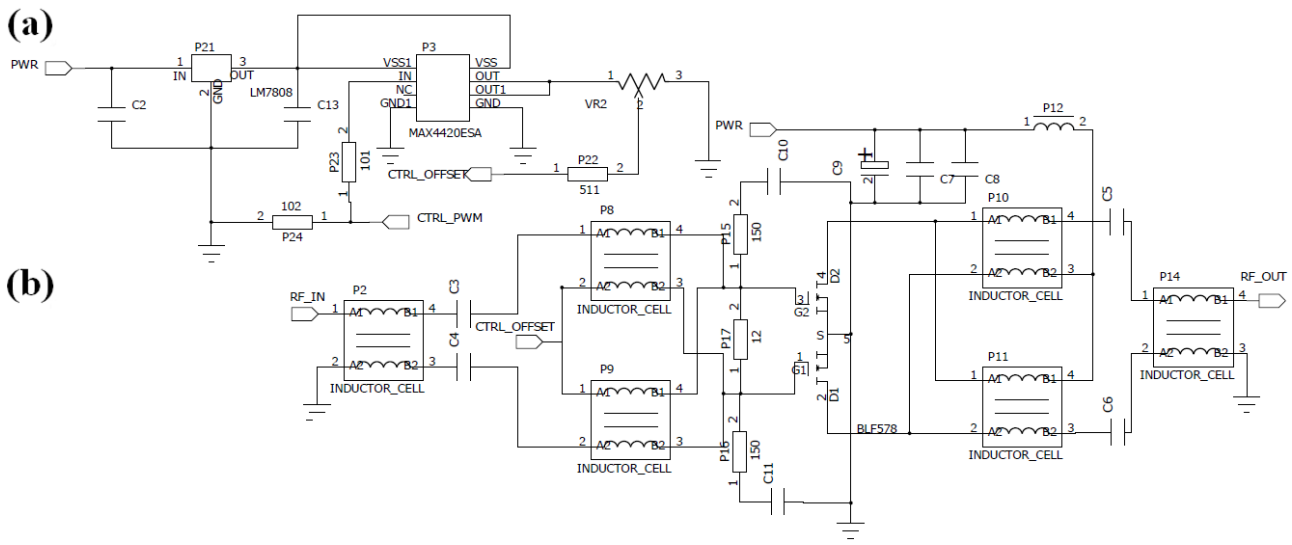

Fig. 2. Schematic of a custom-built power amplifier for ME-IVUS imaging with controlled output: (a) switching-off circuit; and (b) power amplifier.

Instruments) served as the clock source for data acquisition. The ultrasound data were transferred to a computer via a USB 3.0 interface (CYUSB3014, Cypress, San Jose, CA).

C. Transducer

The proposed system is able to connect different kinds of ultrasound catheters for ME-IVUS applications. Two ultrasound transducers with different center frequencies (30 MHz and 60 MHz) were fabricated to evaluate the ME-IVUS method. The single ferroelectric PMN-PT crystal has excellent piezoelectric properties (piezoelectric constant d_{33} > 1500 pC/N, electromechanical coupling coefficient k_t >0.55) [21, 22], and so it was selected as the piezoelectric vibrator for the transducer application (Shanghai Institute of Ceramics of the Chinese Academy of Sciences, Shanghai, China) [23]. An ADT 7100 dicing saw (Advanced Dicing Technologies, Israel) was used to cut the piezoelectric materials, and a precision surface grinder was used to grind the piezoelectric crystal. The piezoelectric vibrator with a conductive backing layer (E-solder 3022) was placed in the side of a metal housing. The Au electrodes were sputtered in a magnetron sputtering machine (JS4S-75G, Jinshenweina Technology Company, Beijing, China) on both sides of the PMN-PT single crystal and on the front of the metal housing. This resulted in one side of the single crystal being connected to the metal housing. Epoxy (Epo-Tek 301, Epoxy Technologies, Billerica, MA) was used to secure the two cables to the piezoelectric vibrator and metal housing. The diameter of the metal housing was about 1.0 mm. The size of the transducer element was about 0.8 * 0.8 mm and 0.4 * 0.4 mm for the 30 MHz and 60 MHz transducers, respectively. Parylene C (Specialty Coating System, Indianapolis Inc., IN) was evaporated as the matching layers by a deposition system (PDS 2010, Specialty Coating System, Indianapolis Inc., IN). The measured bandwidth of 30 MHz and 60 MHz transducers are 53% and 44% respectively (shown in Fig. 3). Meanwhile, the insertion loss are -20 dB and -25 dB for these two transducers.

D. Signal Processing and FPGA Implementation

A linear chirp-based modulated excitation method was used in this study. The waveform was a modulated signal that linearly spanned a frequency bandwidth $B = f_e - f_s$, where f_s and f_e are the starting and ending frequencies of the chirp, respectively. The frequency span was set to 20–40 MHz for the 30 MHz transducer and 48–72 MHz for the 60 MHz transducer. If a chirp sweeps from f_s to f_e over a time T, then the chirp waveform is described by [24]:

$$R(\mathrm{t}) = \omega(\mathrm{t}) \times (\cos(2\pi f_s \,\mathrm{t} + a\pi \,\mathrm{t}^2)) \tag{1}$$

The sweep rate equals $(f_e - f_s)/T$ where T is 2.56 μs in both transducers. Fig. 4(a) shows the transmitted waveform with a 60 MHz center frequency with a Tukey window. $\omega(t)$ is a Tukey windowing function:

$$\omega(t) = \begin{cases} \frac{1}{2}\{1+\cos(\frac{2\pi}{r}[t-\mathrm{r}/2])\} & 0 \le t < \frac{r}{2} \\ 1 & \frac{r}{2} \le t < 1-\frac{r}{2} \\ \frac{1}{2}\{1+\cos(\frac{2\pi}{r}[t-1+\mathrm{r}/2])\} & 1-\frac{r}{2} \le t \le 1 \end{cases} \tag{2}$$

where parameter r is the ratio of a cosine-tapered section length relative to the entire window length, with $0 \le r \le 1$ (r was set to 0.15 in this study). Fig. 4(b) shows the waveform for the compression filter, which is a time-reversed chirp waveform convolved with a Chebyshev window. The Chebyshev window is obtained by applying a discrete Fourier transform to the results from N-point equidistant sampling of Chebyshev polynomials on the unit circle:

$$\omega(\mathrm{n}) = \frac{\sum_{m=-M}^{M} W_C^0(\mathrm{m}) \cos(\frac{2\pi}{N}\mathrm{mn})}{\sum_{m=-M}^{M} W_c^0(\mathrm{m})} \tag{3}$$

where $W_c^0(\mathrm{m})$ is the discrete spectrum of the Chebyshev window, and $|n| \le M$, $M = (N-1)/2$, where N is the length of the window function and must be an odd number.

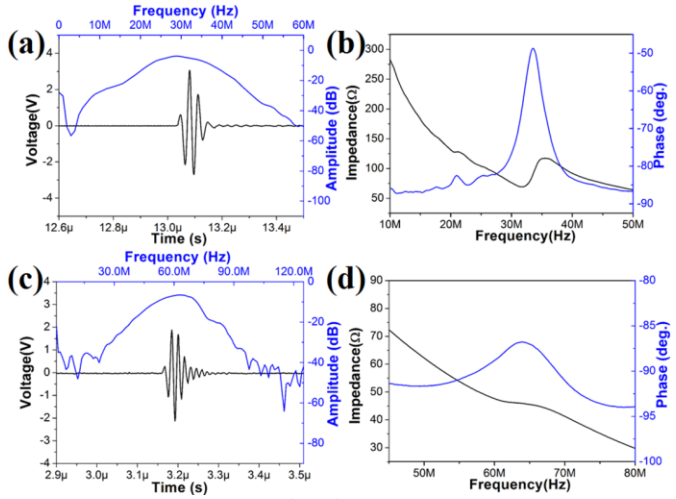

Fig. 3. The acoustic properties of the fabricated transducers. (a) Pulse echo waveform of the 30 MHz transducer; (b) Impedance measurement of the 30 MHz transducer; (c) Pulse echo waveform of the 60 MHz transducer; (d) Impedance measurement of the 60 MHz transducer.

The demodulation method involves performing a convolution between the received chirp echo signal and the compression filter:

$$R_r(\mathrm{t}) * \mathrm{D(t)} = \int_{-\infty}^{\infty} R(\omega)\,\mathrm{D(t-}\omega)\,\mathrm{d}\,\omega \tag{4}$$

where $R_r(t)$ is the received ultrasound echo signal and D(t) is the compression filter. This processing recovered the short-duration pulse, which was similar to the echo signal generated by short-pulse excitation. Fig. 4(c) shows the result obtained in a simulated demodulation process.

Fig. 4(d) shows the block diagram of the algorithms implemented in the FPGA in this study. A fast Fourier transform (FFT)-based method was employed for the convolution process, which reduced the requirements for the logic cell resources and multiplier module. The compression filter was implemented after the bandpass filter in the frequency domain. A complex multiplier was used to perform spectra multiplication after the FFT. The compressed signal was then recovered using an inverse FFT.

E. Evaluation Method

The hardware performance of the system was evaluated first. The waveform generator was characterized by measuring the properties of the waveform using an oscilloscope (Wavepro 715Zi, Teledyne LeCroy, Chestnut Ridge, NY). The electrical impedance of the fabricated transducer was evaluated using an impedance analyzer (4294A, Agilent Technologies, Santa Clara, CA). A pulser-receiver (5800PR, Olympus, Tokyo, Japan) and a steel reflector were employed to measure the bandwidth, where the reflector was placed in a tank of deionized water. The echo waveform was displayed on and recorded by the digital oscilloscope.

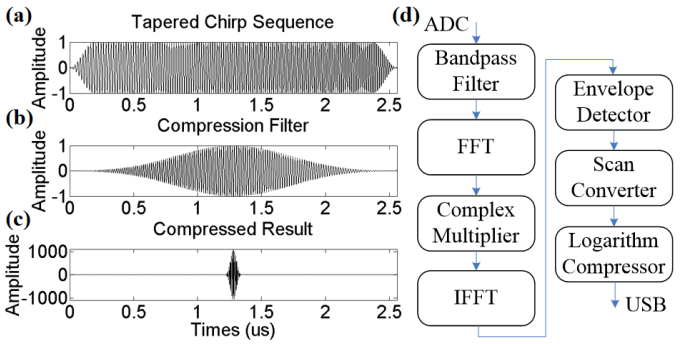

Fig. 4. Signal processing algorithms and FPGA implementation: (a) excitation waveform, (b) compression filter, (c) recovered short-duration pulse after the convolution process, and (d) block diagram of the algorithms implemented in the FPGA specifically for ME-IVUS applications.

A wire phantom and a tissue phantom were fabricated to evaluate the imaging performance. The wire phantom consisted of four tungsten wires with a diameter of 15 μm (Qingyuan Metal Material Inc., Xingtai, Hebei Province, China) in a parallel arrangement separated by 2.5 mm. The axial and lateral resolutions as well as the SNR of the wire phantom were assessed quantitatively.

In addition, a cylindrical agar-based phantom that included three anechoic holes was fabricated. The phantom could produce tissue-mimicking attenuation and backscattering for evaluating the penetration depth and contrast-to-noise ratio (CNR). The attenuation coefficients of the tissue phantom are 30 dB/cm and 98 dB/cm for 30 MHz and 60 MHz respectively. To evaluate the penetration depth, the magnitude of the water echo signal before the phantom was normalized to 0 dB as a reference. The penetration depth was defined as where in the phantom the signal magnitude was reduced by more than 6 dB. Three anechoic holes with different diameters (0.9 mm, 1.4 mm, and 3.0 mm) were fabricated separately and spaced equally at 120 degrees around the center of the phantom. The CNR of the anechoic hole provides an indirect characterization of the device spatial resolution in all directions simultaneously [14]. The CNR was calculated as

$$CNR = \frac{|mean_t - mean_n|}{\sqrt{sta_t^2 + sta_n^2}} \tag{5}$$

where $mean_t$ and $mean_n$ are for the mean magnitudes for the cylindrical tissue-mimicking phantom and the anechoic hole, respectively, while sta_t and sta_n are the corresponding standard deviations. The CNR was calculated three times for anechoic holes of different sizes.

The transducer was placed inside the object to be imaged, which was immersed in a water tank during the experiment. Circumferential scanning was achieved by rotating the water tank using a step motor while the probe remained still. The imaging performance of the proposed ME-IVUS method was evaluated by comparison with traditional short-pulse IVUS. Single-cycle bipolar pulses with center frequencies of 30 MHz and 60 MHz were used for the excitation. The imaging receiver was the same for short-pulse imaging and modulated excitation imaging. To ensure a fair comparison, the amplitudes of the short-pulse and chirp excitation waveforms were set to 60 Vpp (Single cycle bipolar pulse) and 30 Vpp (2.56 μs), respectively, which meant that the spatial peak temporal peak intensities were similar for the two waveforms [25].

An *in vitro* swine aorta specimen was used to evaluate the imaging performance. During the experiment, the probes were inserted into the specimen to perform cross-sectional imaging.

Each image was composed by 1000 A-line ultrasound data.

III. Results

The prototype of the proposed ME-IVUS system is shown in Fig. 5. It consists of a programmable imaging receiver, high-frequency transducer, waveform generator with a compact RF power amplifier, and console software running on a computer. The imaging receiver is an eight-layer PCB incorporating low-noise front-end electronics, ADC, FPGA, and USB 3.0 interface.

A. Electrical Performance of the System

The hardware performance of the system was tested according to the evaluation scheme presented in Section II. The system is able to generate a linear high-voltage waveform from 20 MHz to 80 MHz into a 50-ohm load. The power amplifier could produce a waveform with an amplitude exceeding 60 Vpp, with the frequency range covering most applications of the ME-IVUS. The speed of data transfer is higher than 100 MB/second for a USB 3.0 interface, which facilitated high-speed imaging performance: >30 frames/second at an image size of 512×512 pixels.

B. Imaging Evaluation with Wire Phantom

Fig. 6 presents images of the wire phantom obtained using different imaging strategies. The images are displayed with a dynamic range of 45 dB, with no background noise. The pattern of the wires could be clearly delineated. The axial resolutions measured at 6.3 mm for 30 MHz pulse and chirp are 60 and 67.5 μm respectively. The lateral resolutions measured for 30 MHz pulse and chirp are 405 and 247.5 μm respectively. Similarly, the value for 60 MHz are 30 and 37.5 μm for axial direction, and 180 and 150 μm for lateral direction. The SNRs for short-pulse excitation and modulated excitation were 43.6 dB and 56.7 dB, respectively, at 30 MHz, and 46.7 dB and 56.3 dB at 60 MHz, clearly indicating that the SNR improved when using the modulated excitation imaging method.

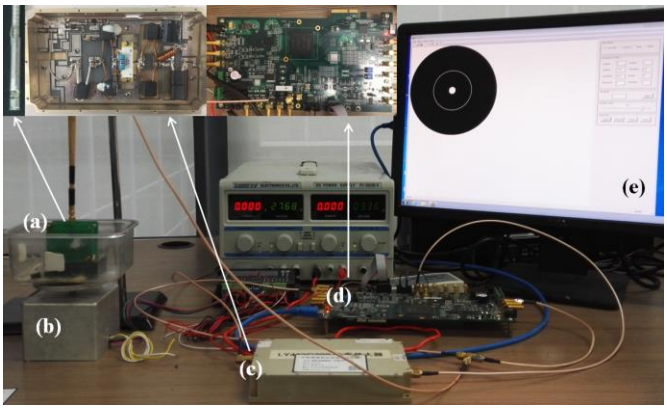

Fig. 5. Prototype of the proposed ME-IVUS system: (a) transducer catheter, (b) motor, (c) power amplifier, (d) image processing receiver, and (e) customized console software.

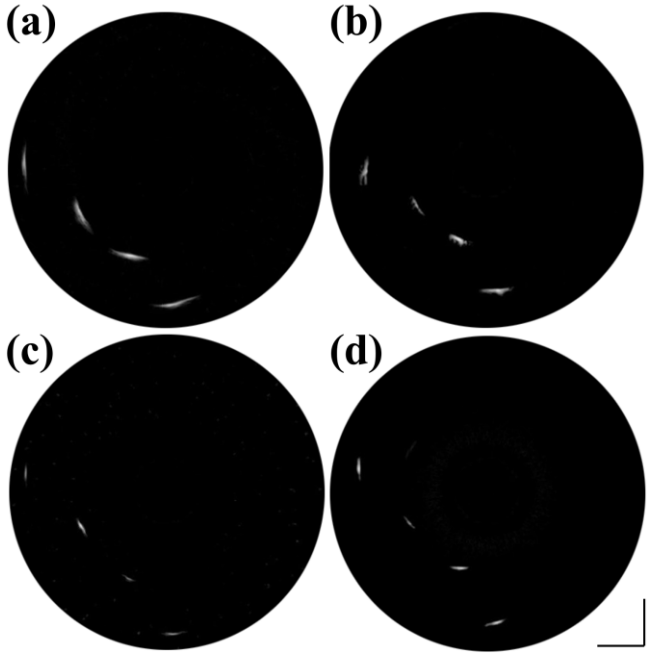

Fig. 6. Images of the wire phantom: (a) 30-MHz short pulse, (b) chirp waveform with 30-MHz center frequency, (c) 60-MHz short pulse, and (d) chirp waveform with 60-MHz center frequency. Scale bars: 2 mm. Dynamic range: 45 dB.

C. Imaging Evaluation by Tissue Phantom

Fig. 7 shows ultrasound images of the tissue phantom. Fig. 7(a,b) show the images acquired using short-pulse imaging and modulated excitation imaging for a central frequency of 30 MHz, while Fig. 7(c,d) show the corresponding images for a center frequency of 60 MHz. As a reference, the magnitude of the water echo signal before the phantom was normalized to 0 dB, and the dynamic range was set to 50 dB for each of the methods. The anechoic holes could be clearly visualized using

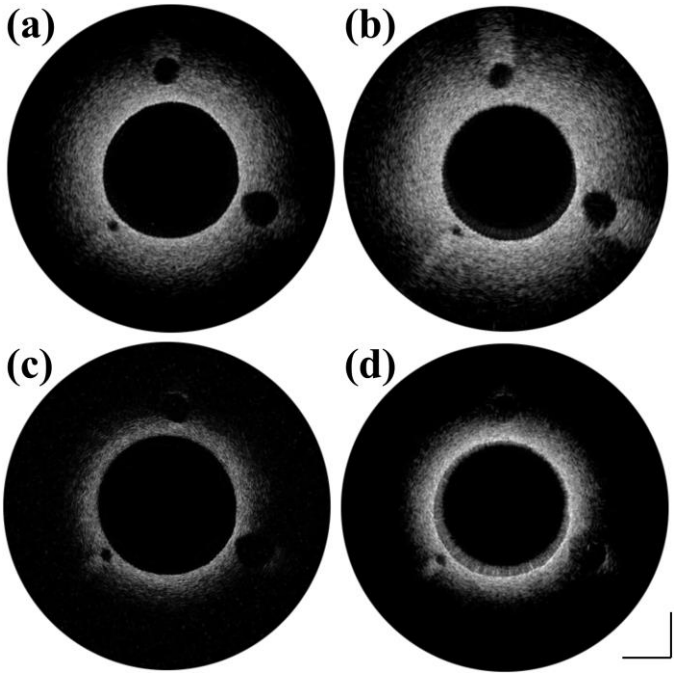

Fig. 7. Sectional images of the tissue phantom acquired using the proposed system: (a) 30-MHz short pulse, (b) 30-MHz chirp, (c) 60-MHz short pulse, and (d) 60-MHz chirp. Scale bars: 5 mm. Dynamic range: 45 dB.

the proposed system. The mean CNRs were 3.0, 3.6, and 4.4 for anechoic holes with diameters of 0.9 mm, 1.4 mm, and 3.0 mm, respectively. Fig. 8 shows the mean backscatter as a function of depth of the tissue phantom. The penetration depth (i.e., where the signal magnitude reduced by more than 6 dB) was improved significantly when using the modulated excitation imaging technique compared with the short-pulse imaging technique for both 30-MHz ultrasound (10.3 mm and 7 mm, respectively) and 60-MHz ultrasound (about 5.6 mm and 3 mm). The results show that the proposed system was able to provide increases of 47.1% and 86.7% in penetration depth for 30 MHz and 60 MHz IVUS respectively.

D. *Imaging of Blood Vessels in vitro*

A normal swine thoracic aorta specimen was used to evaluate the system *in vitro*. The transducer was inserted into the specimen to allow cross-sectional imaging. Ultrasound images of an aorta fixed in a water tank are shown in Fig. 9, which indicate that the penetration depth was greatly improved by using the chirp-based modulated excitation technique at both ultrasound frequencies (Increases of more than 41% and 63% in penetration depth for 30 MHz and 60 MHz IVUS respectively), while the quality of the images was maintained.

IV. Discussion

Progress in cardiovascular research is often driven by advances in tools and methodologies. For example, the development of stents for inserting into an artery with a pathologically narrowed structure due to atherosclerosis allowed a minimal invasive procedure to replace open coronary surgery. Intravascular imaging methods including IVUS have been proposed for visualizing the vessel along the same catheter path used for stent placement. These methods provide important information for guiding stent placement and treatment evaluation. Novel methods of IVUS including elastography and virtual histology were proposed for expanding the applicability of IVUS. High-frequency (>50 MHz) ultrasound has also been proposed for improving

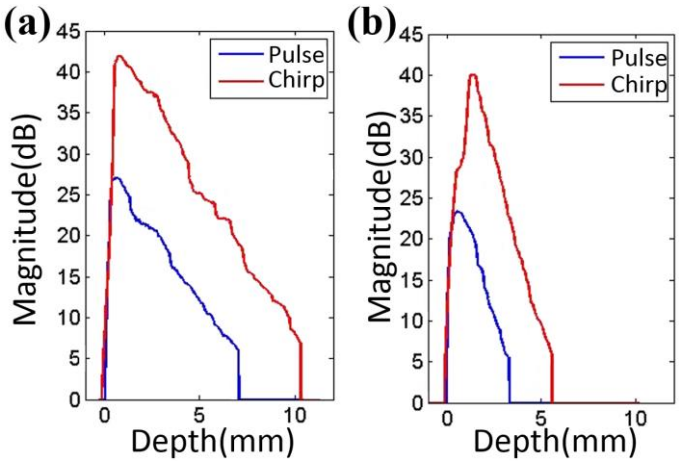

Fig. 8. Mean backscatter as a function of depth of the tissue phantom at (a) 30 MHz and (b) 60 MHz.

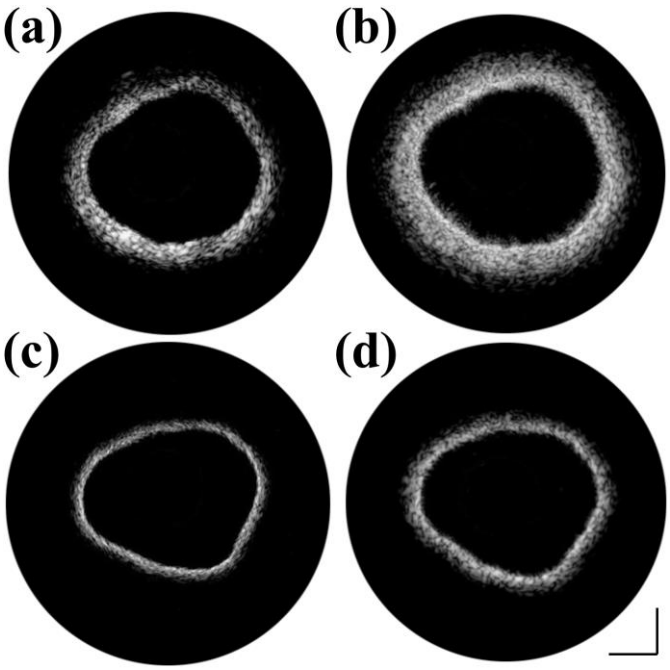

Fig. 9. Images of a swine aorta specimen *in vitro* acquired using the proposed system: (a) 30-MHz short pulse, (b) 30-MHz chirp, (c) 60-MHz short pulse, and (d) 60-MHz chirp. Scale bars: 2 mm. Dynamic range: 45 dB.

the imaging resolution, but this approach is restricted by the associated greater acoustic attenuation.

This paper presents a new IVUS system based on a modulated excitation imaging method. Quantitative measurements demonstrated that the SNR and penetration depth were increased significantly: there was an improvement in the SNR of about 12 dB, while the penetration depth increased by 47.1% for the 30 MHz chirp ultrasound and 86.7% for the 60 MHz chirp ultrasound, clearly demonstrating good system performance. It would be an alternative method to see deep of the tissue with the state-of-the-art catheter. Hydrophone scan was performed with a 3D ultrasound intensity measurement system (UMS3, Precision acoustics, Dorchester, UK). The peak acoustic pressure for 30 MHz IVUS transducer is about 9 KPa. There is no data for 60 MHz probe as the hydrophone in our lab can only cover up to 40 MHz ultrasound frequency. It can be predicted that the acoustic pressure is lower than 9 KPa for 60 MHz transducer.

The transducers in this work were small size with flat shape. The ultrasound beam were diverging which therefore the lateral resolution will be decreased as the depth increased. In addition, the transducers were not exactly perpendicular with the wires which may induce different echo signal during the measurement. Moreover, the demodulation process might improve the lateral resolution in terms of 30 MHz chirp IVUS.

The noise from power amplifier could saturate the ADC during the data acquisition period. Since high frequency ultrasound is sensitive to the noise, we have to switch-off the power amplifier to low down the power noise. In terms of the amplifier itself, the bandwidth of the power is adjusted to 20-90 MHz with +/-3 dB gain fluctuation. The maximum voltage of the waveform is higher than 100 Vpp.

The proposed system may be used for contrast-enhanced

imaging as well to visualize the vasa vasorum, since the ultrasound excitation waveform and the FPGA are programmable to allow different image processing algorithms to be implemented. The system could also be used for ultrasound imaging at higher frequencies.

V. Conclusion

A novel ultrasound system has been proposed and evaluated specifically for ME-IVUS, with the underlying methods, system design, and imaging results presented in detail. The SNR and penetration depth are increased significantly when using the proposed system. Test results show that the proposed system is flexible, and suitable for different applications with a modulated excitation intravascular imaging method, which could potentially increase the usefulness of ultrasound in assessments of cardiovascular diseases.

References

[1] B. N. Potkin, A. L. Bartorelli, J. M. Gessert, R. F. Neville, Y. Almagor, W. C. Roberts, and M. B. Leon, "Coronary artery imaging with intravascular high-frequency ultrasound," Circulation, vol. 81, pp. 1575–85, May 1990.

[2] M. Hartmann, J. Huisman, D. Bose, L. O. Jensen, P. Schoenhagen, G. S. Mintz, R. Erbel, and C. von Birgelen, "Serial intravascular ultrasound assessment of changes in coronary atherosclerotic plaque dimensions and composition: An update," Eur. J. Echocardiogr., vol. 12, no. 4, pp. 313–21, 2011.

[3] J. Aoki, A. C. Abizaid, P. W. Serruys, A. T. Ong, E. Boersma, J. E. Sousa, and N. Bruining, "Evaluation of four-year coronary artery response after sirolimus-eluting stent implantation using serial quantitative intravascular ultrasound and computer-assisted grayscale value analysis for plaque composition in event-free patients," J. Am. Coll. Cardiol., vol. 46, pp. 1670–6, Nov. 1, 2005.

[4] P. A. Lemos, F. Saia, J. M. R. Ligthart, C. A. Arampatzis, G. Sianos, K. Tanabe, A. Hoye, M. Degertekin, J. Daemen, E. McFadden, S. Hofma, P. C. Smits, P. de Feyter, W. J. van der Giessen, R. T. van Domburg, and P. W. Serruys, "Coronary restenosis after sirolimus-eluting stent implantation: Morphological description and mechanistic analysis from a consecutive series of cases," Circulation, vol. 108, no. 3, pp. 257–60, 2003.

[5] A. V. Finn, M. Nakano, J. Narula, F.D. Kolodgie, and Virmani R, "Concept of vulnerable/unstable plaque," Arterioscler Thromb Vasc Biol vol. 30, pp. 1282–92, 2010.

[6] W. E. Hellings, W. Peeters, F. L. Moll,S. R. Piers, J. van Setten, P. J. Van der Spek, J. P. de Vries, K. A. Seldenrijk, P. C. De Bruin, A. Vink , E. Velema, D. P. de Kleijn, and G. Pasterkamp, "Composition of carotid atherosclerotic plaque is associated with cardiovascular outcome: a prognostic study," Circulation, vol. 121, pp. 1941–50, 2010.

[7] C. L. de Korte, and A. F. van der Steen. "Intravascular ultrasound elastography: an overview," Ultrasonics, vol. 40, S1-8, pp. 859-65, May, 2002.

[8] E. S. Shin, H. M. Garcia-Garcia, and P.W. Serruys. "A new method to measure necrotic core and calcium content in coronary plaques using intravascular ultrasound radiofrequency-based analysis," Int J Cardiovasc Imaging, vol. 26, no. 4, pp. 387-96, Apr, 2010.

[9] X. Li, J. Li, J. Jing, T. Ma, S. Liang, J. Zhang, D. Mohar, A. Raney, S. Mahon, M. Brenner, P. Patel, K. K. Shung, Q. Zhou, and Z. Chen." Integrated IVUS-OCT imaging for atherosclerotic plaque characterization," IEEE journal of selected topics in quantum electronics. vol. 20, no. 2, 7100108, 2014.

[10] J. Yuan, S. Rhee, and X. Jiang, "60 MHz PMN-PT based 1-3 composite transducer for IVUS imaging", 2008 IEEE Ultrasonics Symposium, pp. 682-5, 2008.

[11] X. Li, T. Ma, J. Tian, P. Han, Q. Zhou, and K. K. Shung, "Micromachined PIN-PMN-PT crystal composite transducer for high-frequency intravascular ultrasound (IVUS) imaging," IEEE Trans Ultrason Ferroelectr Freq Control, vol. 61, no. 7, pp. 1171-8, 2014.

[12] J. Ma, K. H. Martin, P. A. Dayton, X. Jiang, "A preliminary engineering design of intravascular dual-frequency transducers for contrast-enhanced acoustic angiography and molecular imaging," IEEE Trans Ultrason Ferroelectr Freq Control, vol. 61, no. 5, pp. 870-80, 2014.

[13] J. Ma, K. H. Martin, Y. Li, P. A. Dayton, K. K. Shung, Q. Zhou, and X. Jiang, "Design factors of intravascular dual frequency transducers for super-harmonic contrast imaging and acoustic angiography", Physics in Medicine and Biology, vol. 60, no. 9, pp. 3441-57, 2015.

[14] T. Ma, M. Yu, J. Li, C. E. Munding, Z. Chen, C. Fei, K. K. Shung, and Q. Zhou, "Multi-frequency intravascular ultrasound (IVUS) imaging," IEEE Trans Ultrason Ferroelectr Freq Control, vol. 62, no. 3, pp. 97-107, 2015.

[15] J. Mamou, J. A. Ketterling, and R. H. Silverman. "Chirp-coded excitation imaging with a high-frequency ultrasound annular array," IEEE Trans Ultrason Ferroelectr Freq Control, vol. 55, no. 2, pp. 508-13, 2008.

[16] W. Qiu, Y. Yu, F. K. Tsang, H. Zheng, and L. Sun, "A novel modulated excitation imaging system for micro-ultrasound," IEEE Transactions on Biomedical Engineering, vol. 60, no. 7, pp. 1884-1890, 2013.

[17] D. Maresca, K. Jansen, G. Renaud, G. van Soest, X. Li, Q. Zhou, N. de Jong, K. K. Shung and A. F. W. van der Steen, "Intravascular ultrasound chirp imaging," Appl. Phys. Lett. 100, 043703, 2012.

[18] H. Shekhar, S. Huntzicker, I. Awuor, and M. M. Doyley. "Chirp-Coded Ultraharmonic Imaging with a Modified Clinical Intravascular Ultrasound System," Ultrasound Imaging, Dec 2015.

[19] D. Maresca, G. Renaud, G. van Soest, X. Li, Q. Zhou, K. K. Shung, N. de Jong, and A. F. van der Steen. "Contrast-enhanced intravascular ultrasound pulse sequences for bandwidth-limited transducers," Ultrasound Med Biol, vol. 39, no. 4, pp. 706-13, 2013.

[20] J. Park, X. Li, Q. Zhou, and K. K. Shung. "Combined chirp coded tissue harmonic and fundamental ultrasound imaging for intravascular ultrasound: 20-60 MHz phantom and ex vivo results," Ultrasonics, vol. 53, no. 2, pp. 369-76, 2013.

[21] Q. Zhou, K. H. Lam, H. Zheng, W. Qiu, and K. K. Shung, "Piezoelectric single crystal ultrasonic transducers for biomedical applications," Progress in Materials Science, vol. 66, pp. 87-111, Jun, 2014.

[22] Y. Chen, K. H. Lam, D. Zhou, Q. Yue, Y. Yu, J. Wu, W. Qiu, L. Sun, C. Zhang, H. Luo, H. L. W. Chan, and J. Dai, "High performance relaxor-based ferroelectric single crystals for ultrasonic transducer applications," Sensors, vol.14, no. 8, pp. 13730-58, Jul, 2014.

[23] H. Luo, G. Xu, P. Wang, H. Xu, and Z. Yin, "Compositional homogeneity and electrical properties of lead magnesium niobate titanate single crystals grown by a modified Bridgman technique," Jpn. J. Appl. Phys. vol. 39, no. 9 , pp. 5581–5, 2000.

[24] R. Y. Chiao and X. Hao, “Coded excitation for diagnostic ultrasound: a system developer’s perspective,” IEEE Trans. Ultrason., Ferroelectr., Freq. Control, vol. 52, no. 2, pp. 160–70, Feb. 2005.

[25] M. O’Donnell, "Coded excitation system for improving the penetration of real-time phased-array imaging systems," IEEE Trans. Ultrason., Ferroelect., Freq. Contr., vol. 39, no. 3, pp. 341–51, May 1992.